

# Dynamical neighbors: phase and jamming transitions in hard-spheres fluids

L. Aramis de Icaza Astiz\* and Atahualpa S. Kraemer†

Physics Department, Faculty of Science, Universidad Nacional Autónoma de México, Ciudad Universitaria, México D.F. 04510, Mexico

(Dated: July 5, 2022)

We introduce the concept of dynamic neighbors. This concept defines an order parameter with which phase transitions and jamming can be detected in fluids of hard-spheres without considering orientational or translational symmetry. It also gives a method to estimate the configurational entropy of the system. Using molecular dynamics simulations, we measure the number of dynamic neighbors. With this, it is possible to detect three phases in 2-dimensional system and two phases in the 3-dimensional version. In the hard disk system, these regions correspond to the fluid, hexatic and solid phases, while in the 3-dimensional case, they correspond to the solid and fluid phase. We observe a continuous transition in the 2-dimensional system and a first-order phase transition in the 3-dimensional case. We also observe only two “states” in the case of binary mixtures and for hard-spheres with a fast compression speed. These two states correspond to fluid and jammed states.

PACS numbers:

The study of fluids of particles with hardcore potential has led to an understanding of the mechanisms by which phase transitions occur [1], including transitions to quasicrystalline systems [2, 3], but it has also served to better understand the glass transition [4] via the jamming transition. As simple as hard-sphere models may seem, there is still debate about the kind of transition they present, and their study opened the doors to the Kosterlitz-Thouless-Halperin-Nelson-Young (KTHNY) theory which allowed the recognition of topological phases [5–7]. Unfortunately, until now, this theory has not been generalized for higher dimensional systems; although there have been some efforts [8].

This theory predicted the existence of a phase transition before the crystalline phase in hard disk fluids, known as the *hexatic phase* [9]. However, there is still discussion on the type of transition between the fluid phase and the hexatic phase [10]. The KTHNY theory predicts that this transition should be continuous [5–7, 9]. In contrast, recent numerical experiments conclude that the transition is of first-order [11–14], and this was measured experimentally [15, 16], with no theoretical explanation.

On the other hand, the jamming transition in hard-sphere fluids is still a matter of discussion due to the lack of agreement on the type of transition that occurs [17]. Two types of systems are usually used to study this kind of transition: (i) 3D or higher-dimensional monodisperse systems [18–23] and (ii) 2D mixtures particles of two different sizes [20, 24, 25]. However, sometimes it has been used in 2D monodisperse systems [26]. In the 2-dimensional case, it has been shown that the system does not crystallize when the ratio in the area between the large and small particles is approximately 2:1, and the ratio of particles is 1:2 [24]. While for the 3-dimensional case, crystallization depends on the rate of compression [20].

The first step in studying a phase transition is to define an order parameter that determines when the system is in

one phase or another [27]. In the case of hard-sphere systems, the orientational order parameter is usually used [28]. This parameter locally compares the geometry of the fluid with that of a periodic array. For example, in 2 dimensions, it is usually compared with a triangular arrangement with 6-fold symmetry [11–13, 29–31], while in 3-dimensions, it is usually compared with an FCC arrangement [32–34]. In both cases, the geometry structures with which it is compared are those of maximum density [21, 35]. This order parameter requires defining the close neighbors. As far as we have been able to review, there are two ways in which close neighbors are usually defined in hard-sphere systems: (i) using Voronoi cells [10, 30] and (ii) as a function of distance [12, 13, 29, 31, 34]. Although the system has no apparent rotational or translational symmetry in a jammed state, locally, the orientational order parameters are relatively high, so they are also used to characterize the jamming transition [24].

In this work, we propose to define *dynamical neighbors* as those where there is an interaction between the particles, i.e., two particles are neighbors if they collide with each other. We measure the number of dynamical neighbors as a function of the density. With this, we are available to compute an order parameter independent of the geometry of the densest array and the configurational entropy of the system in a more straightforward way.

## I. MODEL

Although most of the ideas presented here can be used for hard particles of any form, we did our simulations on hard-spheres fluids. The systems we study in this paper are: (i) Single size discs in 2D; (ii) binary mixture of disks with radii 1 and  $\sqrt{2} \sim 1.4$ , with a proportion of 2:1; (iii) and one-size spheres in 3D. In all three systems, periodic boundary conditions were applied to reduce the size effects. In the case of the 2-dimensional systems 10,044 disks were used, while in the 3-dimensional system 2,048 spheres were used. We use the *packing fraction*  $\phi$  as the independent variable.

To perform the simulations, we first used the Lubachevsky–

\*Electronic address: aramisdeicaza@ciencias.unam.mx

†Electronic address: ata.kraemer@ciencias.unam.mx

Stillinger algorithm [36] to obtain systems with a certain packing fraction  $\phi$  numerically. Then we used a molecular dynamics algorithm with hard-spheres [37] to evolve the system, both written in Julia [38].

It is common to define an order parameter  $\Psi_n$  that compares the orientational symmetry of the system to one with  $n$ -fold symmetry. In the 2-dimensional case  $n = 6$  is typically used to compare the system with a perfect triangular arrangement and observe at what density there is a jump of this parameter. In the general case, the order parameter  $n$  is defined as:

$$\Psi_n = \frac{1}{N} \sum_{i=1}^N \left\| \frac{1}{Z_i} \sum_{j=1}^{Z_i} e^{in\theta_{ij}} \right\|, \quad (1)$$

where  $Z_i$  is the number of neighbors of the particle  $i$ , and  $\theta_{ij}$  is the angle formed by the segment that joins the particles  $i$  and  $j$  with the horizontal axis. A similar definition is used for the 3-dimensional systems [20]. This definition of the order parameter does not restrict what is considered a neighbor of the particle  $i$ .

## II. DYNAMICAL NEIGHBORS

One of the simplest ways of defining neighbors is to use distances between particles. In this case,  $\Psi_n$  is a function of  $r$ . If  $r$  is too small,  $\Psi_n(r)$  is not well defined because the number of neighbors  $Z(r)$  is zero, but if it is too long,  $\Psi_n(r) \rightarrow 0$ .

In the case of a crystalline system, it is more or less clear which the close neighbors are, but for systems that do not have translational symmetry, it is more difficult to recognize a distance at which the close neighbors can interact.

Alternatively, we can fix the number of neighbors such that the first  $n$  closest particles are considered the neighbors [39]. Choosing the number  $n$  of neighbors is usually compared to an arbitrary structure, such as the array of maximum density, where the neighbors are defined by contact. In the case of monodisperse fluids hard spheres, this structure is the FCC lattice or the triangular lattice for 3 and 2 dimensions, respectively. In these two examples,  $n$  is the same for every sphere; however, the number of neighbors in the maximum density lattice may vary from disk to disk for systems such as mixtures of spheres [40] or even for other shapes such as fluids of tetrahedra [2]. When the number of neighbors in the array of maximum density is not constant (as for example when there is a binary mixture of particles), it is unclear which is the number of neighbors to consider.

Another alternative is to use Voronoi cells [41, 42], defining neighboring particles as those that share one face of their Voronoi cells. This definition has been used to study the topological properties of random close packing [41, 43]. In particular, it can be shown that there is no regular honeycomb with the topological properties of the Voronoi tessellation produced by a random close packing [43], since the cells would have to have faces with approximately 5.12 sides, and each sphere should have 13.6 neighbors. Although a regular tessellation with these characteristics is meaningless, it is possible to have a non-regular tessellation that, on average, has that number of

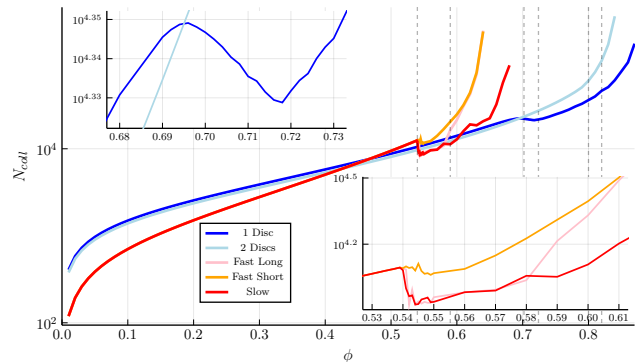


FIG. 1: (Color online) The number of average collisions per particle as a function of  $\phi$  for a system of hard discs of the same size (dark blue), a binary mixture (light blue), hard spheres with a slow compression speed (dark red), a fast compression speed with a short relaxation time (orange), and fast compression speed with a long relaxation time (pink). The insets are the zooms to the phase transition region. The vertical dashed lines correspond to  $\phi = 0.54, 0.59, 0.702, 0.724, 0.8, 0.82$ .

neighbors with that average number of sides per face in each Voronoi cell.

Inspired by this result, Finney [44] obtained the distribution of faces (neighbors) and edges of each face in a random close packing, obtaining on average 14.251 faces per cell and 5.158 edges per face. In addition to the usefulness of studying the topological properties of jammed states, Voronoi cells have also been used to estimate the free volume and thus obtain a heuristic deduction of the Vogel-Fulcher-Tamman law [45, 46]. Moreover, this has laid the foundation for the cage theory used to estimate the densities at which the phase transition occurs [18], and has been used directly to measure the transition between a jamming state and the crystalline phase in hard-spheres when checking the probability of having a certain volume of the Voronoi cell [47].

Despite its usefulness in the description of phase transitions, the definition of a neighbor via a Voronoi cell does not reflect the interactions between particles, and it is expensive computationally [12], especially when the shape of the particles is not spherical [48]. The computational complexity grows fast when we increase the dimension of the system [49].

On the other hand, the number of collisions has been related with pressure via  $\frac{pV}{k_B T} = 1 + \frac{N_{coll}\pi^{1/2}}{9\delta t}$  [50], where  $N_{coll}$  is the number of collisions per particle, and  $\delta t$  is the time window when the collisions occur. In figure 1 we show the average number of collisions as a function of the packing fraction  $\phi$ . The inset plots correspond to the zoom close to the phase transition in the case of 2 and 3-dimensional systems. We can see that the behavior of the average number of collisions as a function of  $\phi$  is similar to the observed pressure [12] close to the phase transition. This observation motivated us to consider the dynamical information that collisions give to define neighbors instead of using geometric information as the distance or the faces of Voronoi cells.

We propose to define the *dynamical neighbors* of a particle

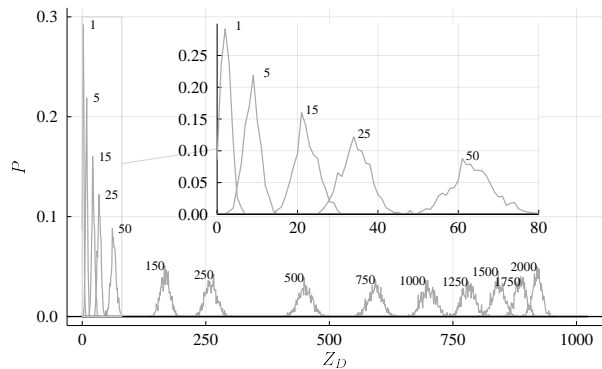


FIG. 2: Distribution of dynamic neighbors  $Z_d$  for a system with 1024 particles at  $\phi = 0.2$  with various values of  $c$ . The labels correspond to the value of  $c$ .

$i$  as the particles that collide with  $i$  in a given time window  $\delta t$ . This implies that the number of dynamical neighbors  $Z_d$  is a function of  $\delta t$ . If the time window is large enough, each particle will have collided with all the others. On the other hand, if the time considered is too short, most of the particles will not collide. This is why it is necessary to define an *adequate* time window, one large enough so that all the particles have collided several times (not necessarily with different particles) but not so long that most have collided with all the particles. As the system is compressed, the energy increases, which means the velocity of particles increases. This means that the distance traveled by each particle in a fixed time window increases as a function of energy. To avoid this problem, we propose that the time window is a function of the kinetic energy  $E$  of the particles  $\delta t(E) = \frac{c}{\sqrt{E}}$ , where  $c$  is a constant.

To choose the proper value of  $c$ , let us first note that unlike neighbors defined using Voronoi cells or as a function of the distance,  $Z_d$  can be very large. We can use this difference in our favor for two reasons: (i) we can produce much wider distributions of neighbors for low densities (specially if  $c$  is large), and extract information from the shape of those distributions, and (ii) we can define a *binding parameter*:  $\mu_{C/Z_d} = \frac{N_{coll}}{\langle Z_d \rangle \sqrt{E}}$  where collisions  $N_{coll}$  is the number of total collision per particle, and  $E$  is the energy of the system. Because this binding parameter is the average number of redundant collisions, it measures a kind of linking intensity between neighbors.

We will use (i) to give a method to choose  $c$ . The distribution of  $Z_d$  depends on  $c$ . Figure 2 shows how the distribution of neighbors changes as a function of  $c$  for  $\phi = 0.2$ . In general, for low packing fractions, the higher the value of  $c$ , the farther the expected value is from 0, and the wider the distribution is. Once the system solidifies, the distribution keeps the same expected value for every  $c$ , but the width of the distribution reduces as  $c$  increases.

Because  $Z_d$  is bounded by the minimum number of neighbors of one particle  $n_m$  in the solid phase and by the number of particles  $N$ , the choice of  $c$  should consider that these boundaries  $N$  and  $n_m$  have little effect. So, we need that the value of  $c$  is large enough such that  $|n_m - \langle Z_d \rangle| \gg \sigma$ , where  $\sigma$  is the

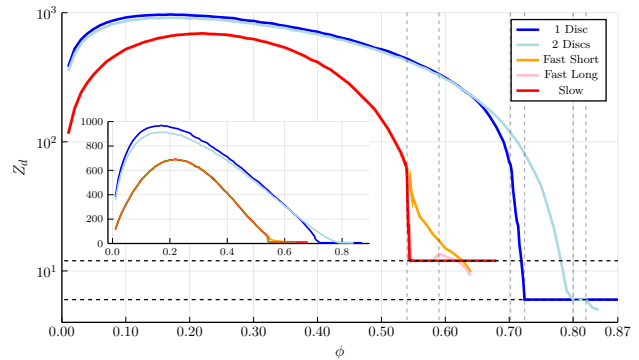


FIG. 3: (Color online) Most probable  $Z_d$  as a function of the packing fraction  $\phi$  for a system of hard discs of the same size (dark blue), a binary mixture (light blue), hard-spheres with a slow compression speed (dark red), a fast compression speed with a short relaxation time (orange), and fast compression speed with a long relaxation time (pink). The insets are the same plot but with no logarithmic scale. The horizontal dashed lines represent 6 dynamic neighbors and 12 dynamic neighbors. The vertical dashed lines correspond to  $\phi = 0.54, 0.59, 0.702, 0.724, 0.8, 0.82$ .

standard deviation of the distribution of  $Z_d$ , but small enough such that  $|N - \langle Z_d \rangle| \gg \sigma$ .

In general, a larger value of  $c$  is better because this means more statistics to obtain the distribution of  $Z_d$ , so, if we are not close to the limit  $\langle Z_d \rangle = N$ , it is better to have a large value of  $c$ . If  $N$  is a large number, it typically is computationally challenging to reach a value of  $c$  such that  $|N - \langle Z_d \rangle| < \sigma$ , so the larger the value of  $c$ , the better.

Because the neighbors distributions are mostly symmetric, unimodal distributions, the position of the maximum, the most probable dynamical neighbor  $Z_d$ , and the average number of neighbors  $\langle Z_d \rangle$  are close related quantities, but they are not identical. Close to a phase transition, the distributions are not perfectly symmetric. In practice  $\langle Z_d \rangle(\phi)$  is smoother than the most probable dynamical neighbor  $Z_d(\phi)$ .

To qualitatively describe the shape of  $Z_d(\phi)$  as a function of  $\phi$ , first note that for the ideal gas  $Z_d(0) = 0$ , since there are no collisions. As the packing fraction increases,  $Z_d$  increases almost linearly (see figure 3). The latter is due to the fact that for low packing fractions most interactions between two given particles occur on a single occasion, then, the mean free path  $\langle l \rangle \propto t_{av} = \delta t N / (2N_{coll})$ , where  $t_{av}$  is the mean time between collisions and  $N$  is the number of particles and also  $\langle l \rangle \propto V / (N v_1(r)) \sim r / \phi$  [51]. The last relation follows since  $v_1(r) \sim v_1'(r)r$ . This implies  $Z_d \sim \langle Z_d \rangle \propto N_{coll} \propto \phi$ . However, if the packing fraction continues to grow, collisions with the same particle (redundant collisions) become common, so the number of dynamic neighbors decreases. So,  $Z_d$  is 0 for  $\phi = 0$ , then grows linearly until redundant collisions become dominant where a maximum is reached and then decreases. When the system crystallizes  $Z_d$  must become 6 or 12 for 2 and 3 dimensions respectively, so we expect an abrupt change in  $Z_d$  as shows figure 3 (solid lines). It can also occur that the system has a jamming transition; in such a case,  $Z_d$  continues to decrease (dashed lines).

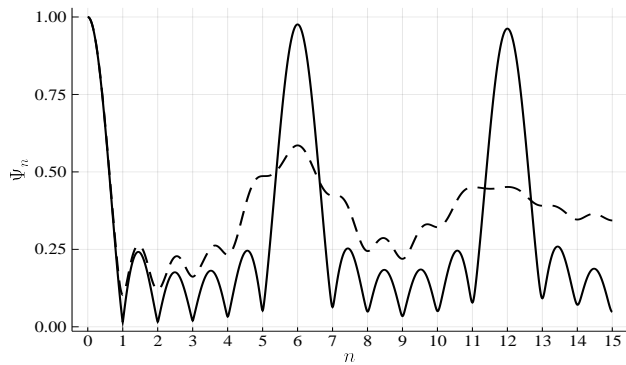


FIG. 4:  $\Psi_n$  as a function of the orientational order  $n$  for the densest arrangement obtained in the monodisperse system (continuous line) and the binary mixture (dashed line). The vertical dashed lines correspond to  $\phi = 0.54, 0.59, 0.702, 0.724, 0.8, 0.82$ .

### A. Diffusion coefficients

Now we would like to focus on the relationship between  $\langle Z_d \rangle$  and the diffusion coefficient. For low densities,  $\langle Z_d \rangle \approx N_{coll}/N$ , since each collision generally occurs with a different particle. However, when the packing fraction grows, this is no longer true. Suppose that only the particle  $i$  can move. The rest have their position fixed. If we tile the space using Voronoi cells omitting the particle  $i$ , for medium and high packing fractions, practically every time the particle  $i$  visits a Voronoi cell, it will collide with the particle in that cell. Thus  $\langle Z_d \rangle$  approximates the number of different Voronoi cells that were visited. Since the average volume of the Voronoi cells is  $V/N$ ,  $\langle Z_d \rangle V/N$  is approximately the volume covered by a particle in time  $\delta t$ , that is, the mean square displacement  $\langle x^2(\delta t) \rangle \sim D\delta t \approx (\langle Z_d \rangle V/N)^{2/d}$ , which implies that  $D \approx (\langle Z_d \rangle V/N)^{2/d} / \delta t$ , where  $d$  is the dimension of the system.

### B. Orientational order parameters

As we have mentioned, another important quantity is  $\mu_{C/Z_d}$ , which can be used as an order parameter without the need to compare with any particular structure, which is a usual problem as discussed in [52].

Before showing that  $\mu_{C/Z_d}$  can be used as an order parameter, we will discuss the typical orientational order parameters using the dynamical neighbors.

We obtained the orientational  $\Psi_n$  for different values of  $n$  both in the monodisperse system of hard disks and in the mixture for  $\phi = 0.88$  for the monodisperse case and  $\phi = 0.84$  for the binary mixture. Figure 4 shows the order parameter  $\Psi_n$ , varying  $n$  from 0 to 15 for the monodisperse (continuous line) and binary mixture (dashed line) systems. As expected, this parameter has peaks around  $n = 6k$ , with  $k$  an integer for the monodisperse case. The other peaks correspond to the cases  $n = k + 1/2$ . These peaks also meet the expectations of equation (1) for a triangular array.

For the binary mixture, it could be expected that the orientational order parameter would depend on the reached configuration. Still, after performing several simulations, almost the same graph was always obtained. In this case, it is notable that  $\Psi_n$  has a maximum for  $n = 6$ , so this parameter can be used to measure the jamming transition, just like in the crystalline case. However, unlike the crystalline case,  $\Psi_5$  and  $\Psi_7$  are not negligible and neither  $\Psi_{11}$ . Therefore, using  $\Psi_6$ , one can expect to see a jump in both cases, while using  $\Psi_5$  and  $\Psi_{11}$ , one should only see a jump when the transition is a jamming transition.

The fact that the orientational order parameter depends on which structure it is compared with has the consequence that there may be an order that we cannot observe for some systems. For example, the maximum density array would appear disordered when measuring the orientational order parameter  $\Psi_5$  as well as a quasicrystal with pentagonal symmetry using  $\Psi_6$ . Instead, we can use an order parameter that is independent of the geometry but depends on the dynamical properties, as is the case of  $\mu_{C/Z_d}$ . If the number of degrees of freedom of the system is reduced, as, during the break of rotational or translational symmetry, we would expect that the number of redundant collisions must change, so  $\mu_{C/Z_d}$  must change its behavior as well.

Figure 5 shows the orientational order parameter  $\Psi_6$  (2-dimensional systems),  $Q_6$  (3-dimensional systems) defined as in [20] and  $\mu_{C/Z_d}$  as a function of  $\phi$  for all the systems we study in this paper. We observe that  $\Psi_6$  and  $\mu_{C/Z_d}$  are very close for the monodisperse hard disk fluid, showing a transition around  $\phi \approx 0.7$ . This result agrees with what was observed using other definitions of close neighbors [53]. For the binary mixture  $\mu_{C/Z_d}$  and  $\Psi_6$  are also similar showing that the jamming transition is around  $\phi \approx 0.75$ .

In the case of 3-dimensional systems  $Q_6$  and  $\mu_{C/Z_d}$  are very different for low packing fractions, but for high packing fractions both parameters are correlated, showing a transition at  $\phi \approx 0.54$ . For the jammed system,  $Q_6$  is very low. It has a small jump before the jamming transition for which we believe is in a region of meta-stability of the fluid and then it goes to 0 while  $\mu_{C/Z_d}$  is always growing, with only a change in the behavior around  $\phi = 0.63$ , which is close to the maximal random jamming.

We can observe that  $\mu_{C/Z_d}$  behaves very close to the orientational order parameter when the orientational order parameter captures a phase or jamming transition but differ when the orientational order parameter does not recognize such transition. So we have an order parameter independent of the final structure we obtain that can be useful if the final structure is unknown, as in a mixture of different size particles or non-spherical particles like tetrahedra [2].

### C. Configurational Entropy

The understanding glass transition is still one of the most critical challenges in material sciences. A possible scenario proposed by Gibbs and Adams [54] relates the increases in viscosity with a dramatic reduction of the number of configu-

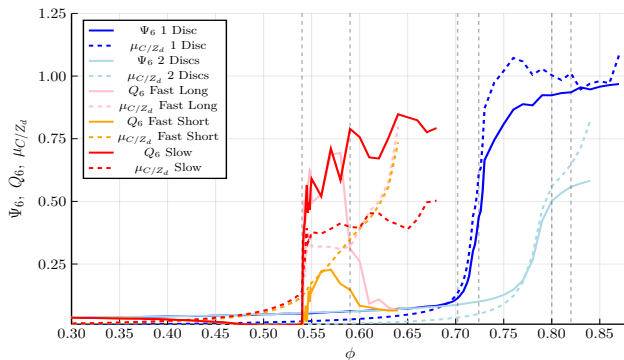


FIG. 5: (color online) Orientational order parameters  $\Psi_6$  and  $Q_6$  (solid lines) and binding parameter  $\mu_{C/Z_d}$  (dashed lines) as a function of the packing fraction for 3-dimensional systems (red-orange lines), and 2-dimensional systems (blue lines). Red and dark blue lines correspond to the systems with a phase transition, while orange and light blue lines represent the systems with a jamming transition. Pink lines correspond to the systems where the compression rate is fast, but the relaxation time is long.

rations available to the fluid. An ideal glass transition occurs if the liquid is trapped in one of the remaining configurations.

Configurational entropy  $s_c$  measures the number of possible distinct states accessible to a system, and it is believed that  $s_c \approx s_L - s_g$  [55, 56], where  $s_L$  is the entropy in the liquid state and  $s_g$  is the entropy of the glassy state. Because in the jammed state, particles are trapped, it is possible to estimate  $s_g$  in single-occupancy cells (SOC) using the Bonding Cell Molecular Dynamics algorithm [57] to measure the average reduced pressure on the walls of each cell  $p_c = P_c V_c / k_B T$  and then obtain the change in free energy as the work of compressing the cells by integrating  $p_c$ . This gives the free energy  $f_g = -s_g$  of the SOC system [57].  $s_L$  can be obtained simply by thermodynamic integration of the equation of state of the fluid (see [58]) from the ideal-gas limit. This algorithm has proved to be accurate [59], but it is admitted to be computationally expensive even if it is already an improvement to other similar algorithms [60]. The reason is that reducing the volume of the cells must be very slow because when the size of the cell is close to the radius of the particles, the number of collisions increases exponentially.

There are at least two other approaches to estimate  $s_c$ , by approximating it with the entropy of only two-particle interactions [61] and using the Shannon entropy of information [62]. The first of these approaches uses the expansion of the entropy in a series of n-particle correlation functions [63]. The correlation function for three or more particles is difficult to calculate, but the pair correlation function is not difficult to estimate via computational simulations. The second approach is based on data compression algorithms. Walraven et al. proposed to store the information of a hard-sphere system in a file, as the positions of the particles, then apply a compression algorithm to the data to obtain a smaller file. The compression ratio (the ratio of file sizes before and after compression) is related to the information entropy of the file, which must be related to the configurational entropy of the system. Ap-

plying this idea to a 3-dimensional hard-sphere system of 256 particles, they obtained an almost constant entropy for packing fractions between 0 and 0.5. Then they observe an abrupt reduction in the entropy similar to what has been observed in [55].

The problem with the approach using the two-particle approximation is that no phase transition is observed, so higher terms are necessary. In the case of the data compression algorithms, they depend on the used algorithm, and the behavior for very high packing fraction seems to move away from the true entropy.

Here we propose an alternative method to estimate the configurational entropy that can be easily obtained for any hard-potential particles.

If the packing fraction is high enough, practically all visits to a Voronoi cell involve a collision with the particle in that cell. Then, the probability that a particle visits  $Z_d$  of neighbors in a time  $\delta t$  depends on the local configuration of particles. So, the standard deviation  $\sigma$  of the distribution  $\rho_\phi(Z_d)$  must be proportional to the number of local configurations, i.e., the number of different local arrays of particles in the system. We assume that this distribution of local arrays is proportional to the number of accessible configurations.

Then the number of configurations  $\Omega(\phi)$ , must be proportional to the standard deviation  $\sigma$  of the probability distribution  $\rho_\phi(Z_d)$ . If the probability distribution of  $Z_d$  is a normal distribution, then, to estimate  $\sigma$ , we just need to calculate the value of the maximum  $\max(\rho_{Z_d})$ , since  $\sigma \sim 1/\max(\rho_{Z_d})$ . Now, using the Boltzmann equation for the entropy we can be calculated  $s_c$  as  $s_c = K_B \log(\Omega)$ , then  $s_c \sim -\log(\max(\rho_{Z_d}))$ .

Figure 6 (top-left) shows the probability distributions of the number of dynamic neighbors for various packing fractions for monodisperse hard disk fluid. In general increasing  $\phi$  increases  $\max(\rho_{Z_d})$ ; however, for  $\phi \in [0.7, 0.72]$  there is a drop in  $\max(\rho_{Z_d})$ . The range of values for which there is this decrease in  $\max(\rho_{Z_d})$  corresponds to the packing fractions of the hexatic phase [12, 13, 29].

A similar effect is observed in figure 6 (bottom-left), where the crystallization process of the fluid of 3-dimensional hard-spheres is shown. However, in this case, there is a jump in the average number of neighbors (it passes from 60 to 12).

In the case of the binary mixture and the fast compression speed, crystallization is frustrated and no fall appears in the maximum of the probability distribution for medium densities. This is shown in figure 6 (top-right), and (bottom-right).

With the height of these distributions, we computed the entropy of the system using  $s_c \approx -\log(\max(\rho_{Z_d}))$ . This is shown in figure 7. The blue lines correspond to the 2-dimensional systems. The red line correspond to a 3-dimensional system with a slow rate of compression, while the orange line and pink line correspond to a fast rate. The difference between the orange and solid pink is that in one case (orange) the time for relaxation of the system was short (pink) while the other was a long time of relaxation. We can see that the paths with slow and fast relaxation times differ notoriously for  $\phi \in [0.54, 0.59]$  (vertical lines). This shows that the states corresponding to the short relaxation times are meta-stable. However, for  $\phi > 0.59$  both paths almost match.

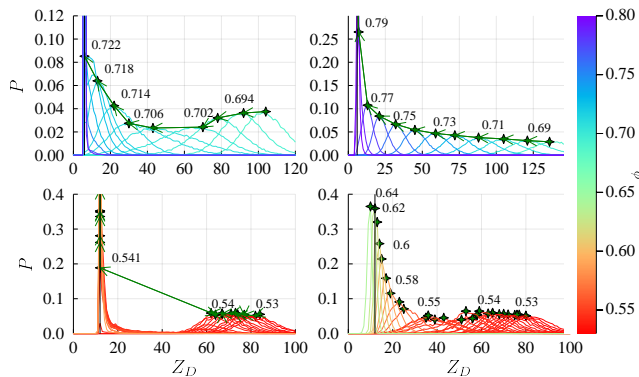


FIG. 6: (Color online) Distributions of the number of dynamic neighbors for various packing fractions for systems: (top-left) monodisperse, and (top-right) binary mixtures of hard discs (bottom-left) slow compression speed and, (bottom-right) fast compression speed of hard spheres. Some labels with the packing fraction were added for easier reading.

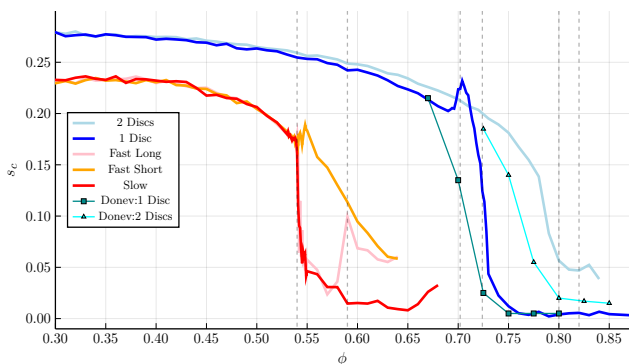


FIG. 7: (color online) Entropy for the 2 and 3-dimensional systems. Blue lines correspond to the 2-dimensional systems, while red and orange lines correspond to the 3-dimensional cases. We added a plot of the configurational entropy minus the entropy of the binary mixture for the 2-dimensional cases, using the data from [55] (green squares for monodisperse systems and blue triangles for binary mixture). The vertical dashed lines correspond to  $\phi = 0.54, 0.59, 0.702, 0.724, 0.8, 0.82$ .

We interpret this to mean that it is at  $\phi = 0.59$  where the jamming transition occurs.

The dark blue curve shows an increment of the entropy just before the phase transition to the crystal phase occurs (similarly the orange curve at the beginning of the meta-stable phase). This increment occurs just before the hexatic phase, which correspond to the lowering of the maximum in the distribution of figure 6 (top-left) at  $\phi = 0.702$ .

We want to highlight that in the 3-dimensional case, the change in entropy when passing from one phase to the other appears discontinuous; that is, it is a first-order transition. However, for the 2-dimensional case, we do not observe that there is an abrupt change in entropy, the hexatic-solid transition, but for the liquid-hexatic transition, there is a jump increasing the entropy, which could be a discontinuity in entropy. This coincides with the abrupt change in the number of

dynamic neighbors for the 3-dimensional system in contrast to what happens in the 2-dimensional case (see inset of figure 3) and would also be in agreement with [12].

About the metastability region  $\phi \in [0.54, 59]$ , it has been suggested that it includes any  $\phi > 0.54$  [64], in such case, there is no glass transition; however, we did not observe that all the systems crystallize.

### III. SOFT PARTICLES AND MONTE-CARLO GENERALIZATIONS

With hard-core potentials, the deviation angle of the particles after a collision is independent of the speed of the particles. Thus, if we consider, for example, only the collisions that produce a minimum deviation, this would be independent of the speed of the particles that collide, and all the measurements would be proportional. Thus, the number of neighbors can be decoupled from temperature independent of any imposition to consider a minimum deviation (for example, at least angles of 45 degrees).

In the case of soft particles, the deviation depends on the speed of the particles. Then, to take this into account, any generalization of the dynamical neighbors to soft potential must rely on the speed of particles that collide. Then the distribution of dynamical neighbors would be temperature-dependent, as well as the entropy or the binding parameter.

On the other hand, in Monte-Carlo simulations, a particle's movement is rejected with some probability if the energy is increased. The rejection can be interpreted as a collision. So, all the particles involved in rejecting a movement can be considered dynamical neighbors. For hard particles, this means every time there is an overlap between particles, but in the case of soft particles, this depends on the temperature.

### Conclusions and remarks

We proposed to define dynamical neighbors in systems with hard-core potential as those that have a collision in a given time window. We found that the average number of dynamical neighbors must be proportional to the diffusion coefficient. Also, we proposed defining an order parameter using the number of collisions and the number of dynamical neighbors. We found that this order parameter, which is independent of the system's geometry, can be used to detect phase and jamming transitions in 2 and 3-dimensions. In 2-dimensions, this parameter was available to see fluid, hexatic, and crystal phases. Finally, we propose a method to estimate the configurational entropy using the distribution of dynamic neighbors. We computed it for four systems: hard disks of a single size of particles, a binary mixture of hard disks, and hard spheres with slow and fast compression rates. The measurements of this entropy were in agreement with other measurements reported in the literature. Since the simplicity of the method, it was possible to measure the entropy in many more packing fractions and with larger systems. This allowed us to observe an increase in the entropy in the transition from fluid to the

hexatic phase and the phase transition from fluid to solid in 3–dimensions. We also observe a meta-stable phase in 3–dimensions and a drop in the entropy during the transition from hexatic to the solid phase. We also observed that the metastable phase becomes stable at a packing fraction corresponding to the jamming transition in 3D.

### Acknowledgments

We thank David P. Sanders for useful discussions. The authors appreciate the computing platform provided by the Lab-

oratorio de Cómputo de Alto Rendimiento, under coordination of Departamento de Matemáticas of Facultad de Ciencias, UNAM.

- 
- [1] B. Alder and T. Wainwright, *Phys. Rev.* **127**, 359 (1962).
- [2] A. Haji-Akbari, M. Engel, A. S. Keys, X. Zheng, R. G. Petschek, P. Palfy-Muhoray, and S. C. Glotzer, *Nature* **462**, 773 (2009).
- [3] D. Wang, T. Dasgupta, E. B. van der Wee, D. Zanaga, T. Altantzis, Y. Wu, G. M. Coli, C. B. Murray, S. Bals, M. Dijkstra, et al., *Nature Phys.* **17**, 128 (2021).
- [4] L. Berthier and G. Biroli, *Rev. Mod. Phys.* **83**, 587 (2011).
- [5] J. M. Kosterlitz and D. J. Thouless, *J. Phys. Condens. Matter* **6**, 1181 (1973).
- [6] B. Halperin and D. R. Nelson, *Phys. Rev. Lett.* **41**, 121 (1978).
- [7] A. Young, *Phys. Rev. B* **19**, 1855 (1979).
- [8] R. Bauerschmidt, D. Conache, M. Heydenreich, F. Merkl, and S. W. Rolles, in *Ann. Henri Poincaré* (2019), vol. 20 Issue 9, pp. 3019–3057.
- [9] D. R. Nelson and B. Halperin, *Phys. Rev. B* **19**, 2457 (1979).
- [10] P. S. Ruiz, Q.-I. Lei, and R. Ni, *Comm. Phys.* **2**, 1 (2019).
- [11] K. Binder, S. Sengupta, and P. Nielaba, *J. Phys. Condens. Matter* **14**, 2323 (2002).
- [12] M. Engel, J. A. Anderson, S. C. Glotzer, M. Isobe, E. P. Bernard, and W. Krauth, *Phys. Rev. E* **87**, 042134 (2013).
- [13] E. P. Bernard and W. Krauth, *Phys. Rev. Lett.* **107**, 155704 (2011), URL <https://link.aps.org/doi/10.1103/PhysRevLett.107.155704>.
- [14] C. H. Mak, *Phys. Rev. E* **73**, 065104 (2006), URL <https://link.aps.org/doi/10.1103/PhysRevE.73.065104>.
- [15] A. L. Thorneywork, J. L. Abbott, D. G. A. L. Aarts, and R. P. A. Dullens, *Phys. Rev. Lett.* **118**, 158001 (2017), URL <https://link.aps.org/doi/10.1103/PhysRevLett.118.158001>.
- [16] P. Huang, T. Schönenberger, M. Cantoni, L. Heinen, A. Magrez, A. Rosch, F. Carbone, and H. M. Rønnow, *Nature Nano.* **15**, 761 (2020).
- [17] G. Biroli, *Nature Phys.* **3**, 222 (2007).
- [18] A. S. Kraemer and G. G. Naumis, *J. of Chem. Phys.* **128**, 134516 (2008).
- [19] C. Estrada and M. Robles, *J. of Chem. Phys.* **134**, 044115 (2011).
- [20] S. Torquato and F. H. Stillinger, *Rev. of Mod. Phys.* **82**, 2633 (2010).
- [21] X.-Z. Wang, *J. Chem. Phys.* **122**, 044515 (2005).
- [22] E. Ustinov, *J. of Chem. Phys.* **146**, 034110 (2017).
- [23] A. L. Thorneywork, D. G. Aarts, J. Horbach, and R. P. Dullens, *Phys. Rev. E* **95**, 012614 (2017).
- [24] A. Donev, F. H. Stillinger, and S. Torquato, *Phys. Rev. Lett.* **96**, 225502 (2006).
- [25] J. Callahan and J. Machta, *Phys. Rev. E* **95**, 063315 (2017).
- [26] S. Torquato and Y. Jiao, *Phys. Rev. E* **82**, 061302 (2010).
- [27] J. Zinn-Justin, *Phase Transitions and Renormalization Group* (Oxford University Press, 2007).
- [28] S. Torquato and F. H. Stillinger, *Rev. Mod. Phys.* **82**, 2633 (2010).
- [29] A. Jaster, *Phys. Lett. A* **330**, 120 (2004).
- [30] A. Jaster, *Phys. Rev. E* **59**, 2594 (1999).
- [31] E. Basurto, C. Haro-Pérez, C. A. Vargas, and G. Odriozola, *Phys. Chem. Chem. Phys.* **20**, 27490 (2018).
- [32] S. Torquato, T. M. Truskett, and P. G. Debenedetti, *Phys. Rev. Lett.* **84**, 2064 (2000).
- [33] P. J. Steinhardt, D. R. Nelson, and M. Ronchetti, *Phys. Rev. B* **28**, 784 (1983).
- [34] G. Odriozola, *J. Chem. Phys.* **131**, 144107 (2009).
- [35] T. Hales, M. Adams, G. Bauer, T. D. Dang, J. Harrison, H. Le Truong, C. Kaliszyk, V. Magron, S. McLaughlin, T. T. Nguyen, et al., in *Forum of Mathematics, Pi* (Cambridge University Press, 2017), vol. 5.
- [36] B. D. Lubachevsky and F. H. Stillinger, *J. Stat. Phys.* **60**, 561 (1990).
- [37] H. Sigurgeirsson, A. Stuart, and W.-L. Wan, *J. Comp. Phys.* **172**, 766 (2001).
- [38] J. Bezanson, A. Edelman, S. Karpinski, and V. B. Shah, *SIAM Rev.* **59**, 65 (2017).
- [39] O. Häggström and R. Meester, *Random Struct Algorithms* **9**, 295 (1996).
- [40] L. Yi, K. J. Dong, R. Zou, and A. Yu, *Powder Technol.* **224**, 129 (2012).
- [41] S. Sastry, D. S. Corti, P. G. Debenedetti, and F. H. Stillinger, *Phys. Rev. E* **56**, 5524 (1997).
- [42] S. Sastry, P. G. Debenedetti, and F. H. Stillinger, *Phys. Rev. E* **56**, 5533 (1997).
- [43] H. Coxeter et al., *Ill. J. Math.* **2**, 746 (1958).
- [44] J. Finney, *Proc. R. Soc. A* **319**, 479 (1970).
- [45] S. R. Elliott, *Physics of amorphous materials* (Longman Group, Longman House, Burnt Mill, Harlow, Essex CM 20 2 JE, England, 1983., 1983).
- [46] D. Wales et al., *Energy landscapes: Applications to clusters, biomolecules and glasses* (Cambridge University Press, 2003).
- [47] Y. Jin and H. A. Makse, *Physica A* **389**, 5362 (2010).
- [48] F. M. Schaller, S. C. Kapfer, M. E. Evans, M. J. Hoffmann, T. Aste, M. Saadatfar, K. Mecke, G. W. Delaney, and G. E. Schröder-Turk, *Philos Mag* **93**, 3993 (2013).
- [49] J.-D. Boissonnat, M. Sharir, B. Tagansky, and M. Yvinec, *Discrete Comput Geom* **19**, 485 (1998).
- [50] L. Woodcock, *Faraday Discuss.* **106**, 325 (1997).

- [51] R. A. Serway and J. W. Jewett, *Physics for scientists and engineers* (Cengage learning, 2018).
- [52] C. E. Zachary and S. Torquato, *J. Stat. Mech. Theory Exp.* **2009**, P12015 (2009).
- [53] A. Huerta and G. G. Naumis, *Phys. Rev. Lett.* **90**, 145701 (2003).
- [54] G. Adam and J. H. Gibbs, *J. of Chem. Phys.* **43**, 139 (1965).
- [55] A. Donev, F. H. Stillinger, and S. Torquato, *J. of Chem. Phys.* **127**, 124509 (2007).
- [56] L. Berthier, M. Ozawa, and C. Scalliet, *J. of Chem. Phys.* **150**, 160902 (2019).
- [57] A. Donev, F. H. Stillinger, and S. Torquato, *J. Comp. Phys.* **225**, 509 (2007).
- [58] S. Luding, *Phys. Rev. E* **63**, 042201 (2001).
- [59] A. Donev, F. H. Stillinger, and S. Torquato, *Phys. Rev. Lett.* **96**, 225502 (2006).
- [60] V. Senthil Kumar and V. Kumaran, *J. of Chem. Phys.* **123**, 114501 (2005).
- [61] A. Baranyai and D. J. Evans, *Phys. Rev. A* **40**, 3817 (1989).
- [62] E. Walraven and F. Leermakers, *Soft Matter* **16**, 3740 (2020).
- [63] R. Nettleton and M. Green, *J. of Chem. Phys.* **29**, 1365 (1958).
- [64] M. Rintoul and S. Torquato, *Phys. rev. lett.* **77**, 4198 (1996).